Wireless Pers Commun
DOI 10.1007/s11277-012-0504-y

Effects of Nakagami-Fading Parameters and Power Control Error on Performance of DS-CDMA Cellular Systems with Adaptive Beamforming

Mohamad Dosaranian-Moghadam · Hamidreza Bakhshi · Gholamreza Dadashzadeh

Abstract It is well known that power control error (PCE) is a critical issue in CDMA cellular systems. In this paper, the bit error rate (BER) of a direct sequence-code division multiple access (DS-CDMA) receiver with imperfect power control, adaptive beamforming, and voice activity is derived in frequency-selective Nakagami fading channels. We discuss the effects of PCE, Nakagami-*m* fading parameter, and channel's multipath intensity profile as average signal strength and rate of average power decay and their effects on the BER performance of DS-CDMA cellular systems. In this paper, the RAKE receiver consists of three stages. In the first stage, with conjugate gradient adaptive beamforming algorithm, the desired users' signal in an arbitrary path is passed and the inter-path interference is canceled in other paths in each RAKE finger. Also in this stage, the multiple access interference (MAI) from other users is reduced. Thus, the matched filter (MF) can be used for the MAI reduction in each RAKE finger in the second stage. In the third stage, the output signals from the MFs are combined according to the conventional maximal ratio combining principle and then are fed into the decision circuit for the desired user. How the Nakagami fading parameters, power control imperfections, or the number of resolvable paths affect the reverse link capacity of the system is discussed in detail. Analytical and simulation results are also given for systems with different processing gains and number of BSs in the cell-selection process with various Nakagami fading parameters.

Keywords Adaptive beamforming · DS-CDMA · Multipath intensity profile · Nakagami fading channel · Power control error · Voice activity

M. Dosaranian-Moghadam (✉)
Department of Electrical Engineering, Qazvin Branch, Islamic Azad University, Qazvin, Iran
e-mail: m_dmoghadam@qiau.ac.ir; m_dmoghadam@yahoo.com

H. Bakhshi · G. Dadashzadeh
Department of Electrical Engineering, University of Shahed, Tehran, Iran

H. Bakhshi
e-mail: bakhshi@shahed.ac.ir

G. Dadashzadeh
e-mail: gdadashzadeh@shahed.ac.ir

Published online: 12 January 2012

1 Introduction

Code-division multiple access (CDMA) for cellular communication networks requires the implementation of some forms of adaptive power control. In the uplink of CDMA systems, the maximum number of supportable users per cell is limited by multipath fading, shadowing, and near-far effects that cause fluctuations of the received power at the base station (BS). The optimum power control law proposed by Gejji [1] has been developed as a function of the distance and the direction from the base station to provide a more accurate power control scheme. Two types of power control are often considered: closed-loop power control and open-loop power control. In an open-loop power control, a mobile set adjusts its transmit power according to its received power in the downlink. Also, in a closed-loop power control, according to the received signal power at a base station, the base station sends a command to a mobile set (MS) to adjust the transmit power of the mobile. Moreover, closed-loop power control is employed to combat fast channel fluctuations due to fading. Closed-loop algorithms can effectively compensate for fading variations when the power control updating time is smaller than the correlation time of the channel. Indeed, if the variability of the radio channel is faster than the control rate, the power control algorithm fails because it refers to old channel estimations, thus causing a power control error (PCE) [2–7].

In a practical system, the control of power is not perfect. The PCE is caused by the power measurement error and the measurement delay in the power control process. Finite dynamic range of transmission is another imperfection in power control. In a practical situation, a mobile set is not able to change its power to any desired value. Hence, the performance of a power control algorithm will be affected by the PCE and the dynamic range of transmission [8]. The issue of the effect of PCEs on CDMA cellular systems has received a great deal of attention over the last few years. In [9,10], analysis on the effect of the PCE has been carried out for the reverse link (uplink). In [11], considering the global influence of the speed of the adaptive power control system, dynamic range of the transmitter, and propagation statistics as fading and shadowing is also given for the reverse link. On the other hand, in [2], the effects of power control imperfections, the number of resolvable paths, or proportion of simultaneous open-loop and closed-loop power controlled users on the reverse link capacity of the CDMA cellular systems are studied. An analysis explicitly considering the interference due to other-cell users can be found in [8] for a system in which shadowing is not considered and users are connected to the nearest base station.

On the other hand, it is generally acknowledged that a viable approach for increasing the capacity of DS-CDMA cellular systems in the reverse link is represented by antenna arrays [12–17]. Literature available on multiple antenna systems for DS-CDMA covers several aspects, such as capacity evaluation, algorithms for array combining, and space-time channel characterization. A key factor to the success of array systems with DS-CDMA is, in particular, the capability of providing good performance even in the presence of moderate near-far effect, i.e., in the presence of less-stringent forms of reverse link power control. Traditionally, base stations use antenna arrays to enhance link performance, but with the rapid advancement of technology, mobile units have recently started to share this advantage. There are two main techniques that are used to exploit transmit antenna arrays. The first one is space-time coding, which provides diversity in fading environments [18]. The second is beamforming, which provides spatially matched transmission or (in multiuser scenarios) mitigates interference [19–22]. The power gain that is achieved by transmit beamforming is proportional to the number of transmit antennas. The goal of adaptive beamformers is to enhance the desired signal and suppress noise as well as strong interferences at the sensor array output simultaneously. In past years, some interesting approaches for adaptive beam-

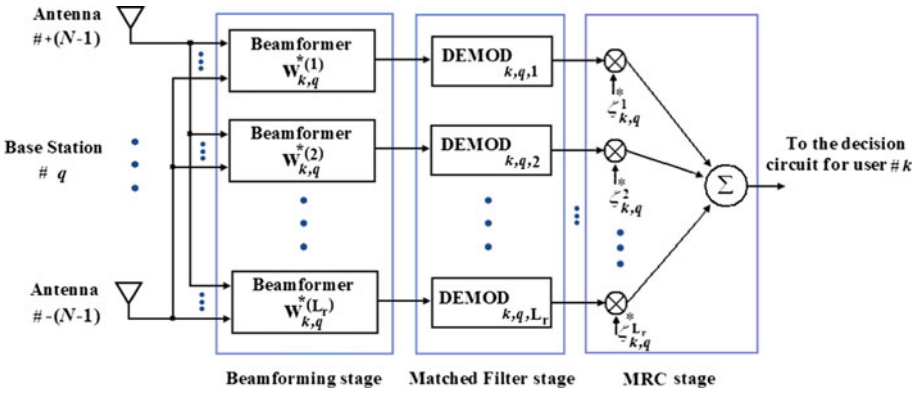

Fig. 1 Block diagram of a three-stage RAKE receiver in DS-CDMA system [26,29]

forming have been suggested to provide robustness against various mismatches in the channel state information for line of sight (LoS) propagation environments, e.g., [22–24]. In addition, the problem of robust beamforming for flat fading channels was considered in [19]. Also, in [25], a new beamforming scheme is proposed which can transmit multiple data streams simultaneously in multiple-input multiple-output (MIMO) channels by generalizing transmit maximal ratio combining technique. Recently, the robustness of transmit beamforming from the worst-case robustness perspective has been studied in [20].

The contribution of this paper is to extend results previously obtained by the authors [26], Efthymoglou et al. [27], and Femenias and Carrasco [3,4] for joint multiple-cell system, adaptive beamforming, and PCE in Nakagami fading channels. Accordingly, in this paper we discuss PCE, processing gain, the number of resolvable paths, the number of BSs in the cell-selection process, and effects of Nakagami fading parameters as Nakagami-m fading parameter, average signal strength, and rate of average power decay and their effects on the BER performance of DS-CDMA cellular systems.

In this work, the performance analysis of direct-sequence (DS)-CDMA system in the presence of Nakagami fading channel has been studied. If the delay spread in a multipath channel is larger than a fraction of a symbol, the delayed components will cause inter-symbol interference (ISI). Adaptive receiver beamforming schemes have been widely used to reduce both co-channel interference (CCI) and ISI and to decrease the bit error rate (BER) by adjusting the beam pattern such that the effective SINR at the output of the beamformer is optimally increased [28].

In this paper, a RAKE receiver in DS-CDMA cellular system is analyzed in three stages according to Fig. 1 [29–32]. In the first stage, this receiver uses conjugate gradient (CG) adaptive beamforming to find optimum antenna weights assuming perfect estimation of the channel parameters (direction, delay, and power) for the desired user. The desired user resolvable paths' directions are fed to the CG beamformer to cancel out the CCI from other directions. Also, the RAKE receiver uses conventional demodulation in the second stage and conventional maximal ratio combining (MRC) in the third stage to reduce multiple-access interference (MAI). Reducing the MAI and the CCI will further decrease the system BER. In this paper, we also use constrained least mean squared (CLMS) algorithm and switched-beam (SB) technique in the first stage of the RAKE receiver.

The rest of the paper is organized as follows. The system model is presented in Sect. 2. The RAKE receiver structure is described in Sect. 3. In Sect. 4, the error performance analysis is

presented. Section 5 describes the CLMS algorithm and the SB technique. Simulation results and comparisons are provided in Sect. 6, and finally the conclusions are presented in Sect. 7.

2 System Model

In this paper, the radio channel is affected by long-and short-term fluctuations. Long-term fluctuations are due to shadowing and distance variations, while short-term fluctuations are due to multipath fading. The channel propagation gain between mobile k and base station q for each path will thus be given by [10]

$$G_{k,q} = \frac{\chi_{F_{kq}}}{d_{k,q}^{L_\alpha}(x, y)10^{\xi_{k,q}/10}} \tag{1}$$

where $d_{k,q}(x, y)$ is the distance between user k and BS q (see Fig. 2); L_α is path-loss exponent; $\xi_{k,q}$ is a random variable modeling the shadowing between user k and BS q, which is assumed to follow a Gaussian distribution with mean 0 and variance σ_s^2 and $\chi_{F_{kq}}$ is a random variable modeling the multipath fading process between mobile k and BS q. We assume that multipath propagation results in the reception of L equal strength paths with Nakagami distribution, and RAKE receiver with $L_r \leq L$ fingers is assumed to optimally combine the individual paths. The power of the multipath fading will thus have a chi-squared distribution with $2L$ degrees of freedom, with probability density function (pdf) [10]

$$f_{\chi_F}(x) = \frac{L^L}{(L-1)!}x^{L-1}e^{-Lx}U(x) \tag{2}$$

where $U(.)$ is the unit step function.

In this paper, we assume that every BS transmits a pilot signal, and MSs connect to the BS whose pilot signal is received with the highest average power level. As a given MS may

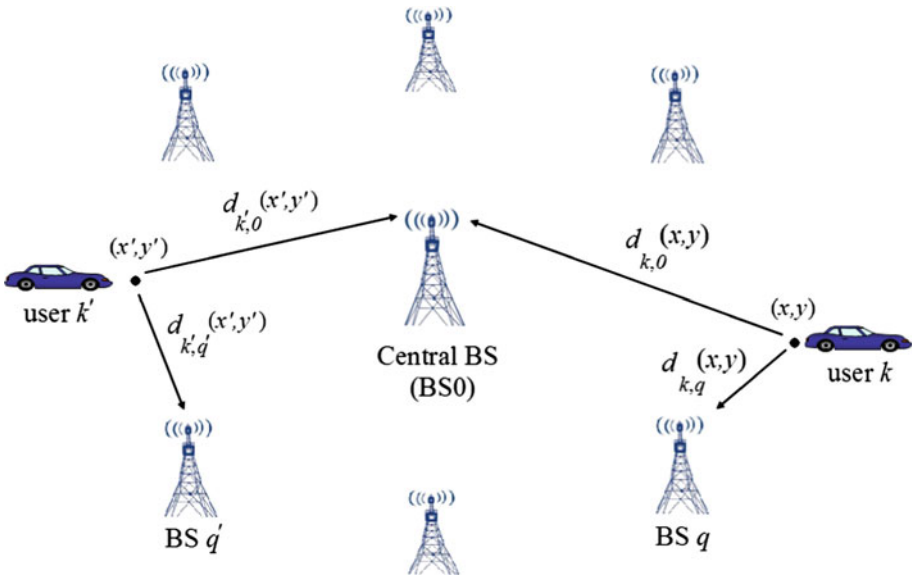

Fig. 2 The distance between mobile transmitters and base station receivers in the reverse link [28]

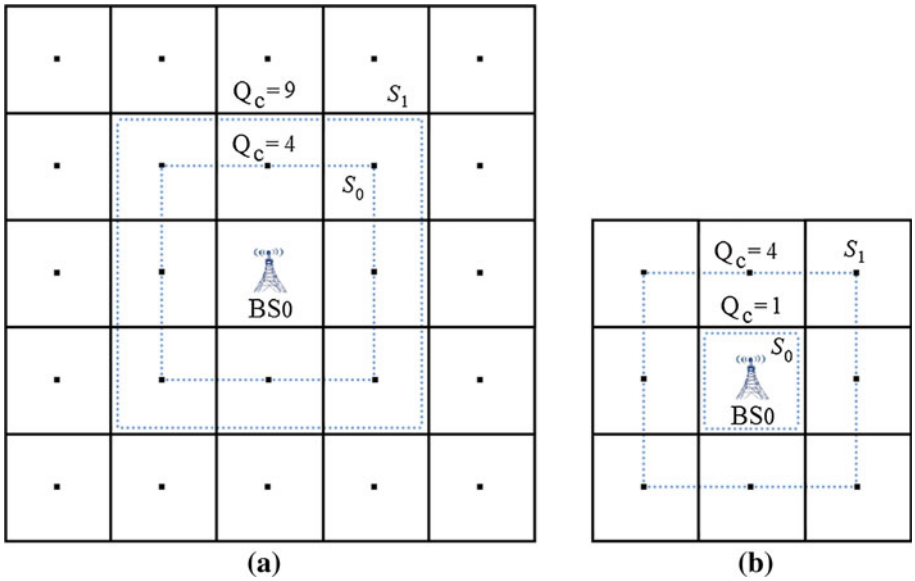

Fig. 3 Cellular system for different values of Q_c [4]

not be able to measure the pilot signals of all the BSs in the system, the selection will be considered as limited to the nearest Q_c BSs can also be justified by the use of neighbor cell lists by MSs, since MSs are regularly provided with a list of handover candidates to be monitored [4,10]. The selection among the nearest Q_c BSs divides the layout in two regions. We denote as S_0 the region of the cellular layout which contains all the points having the central BS (BS0) included among the Q_c nearest stations, while the remaining part of the layout is denoted as S_1. The size and the shape of these regions are a function of Q_c. Figure 3 shows regions S_0 (the area inside the corresponding highlighted polygon) and S_1 (the area outside the corresponding highlighted polygon) that are associated with different values of Q_c.

In this paper, we focus on the uplink communication paths in a DS-CDMA cellular system. The channel is modeled as a frequency selective channel with Nakagami distribution and lognormal distributed shadowing. Initially, we consider L resolvable paths for each link that are optimally combined through a RAKE receiver with $L_r \leq L$ fingers according to Fig. 1. It should be mentioned that in this paper, it is not considered the unresolvable subpaths for each link (see [16] for more details). Also assume that there are M active base stations in the network, with K users connected to each base station. All of the users are assumed to perform open loop power control, also known as slow power control (SPC), in order to compensate for the long-term radio channel path-loss fluctuations due to shadowing and distance variations. Also, in this paper, we assume that each base station uses an antenna array of S sensors and N weights, where $S = 2N - 1$, to receive signals from all users. Note that in CG adaptation algorithm, unlike other adaptation algorithms, the number of weights is less than the number of sensors. Also, for simplicity we assume a synchronous DS-CDMA scheme and BPSK modulation in order to simplify the analysis of the used techniques.

A commonly used model for a frequency-selective multipath channel is a finite-length tapped delay line, where only delays that are multiple integer of the chip duration time are

considered. In this case, the low-pass equivalent impulse response of the band-pass channel for the link between the user k and sensor s of BS q ($1 \leq q \leq M$) can be modeled as [3,33]

$$h_{k,q,s}(t) = \frac{\sqrt{\alpha_c}\sqrt{\chi_{Fkq}}}{d_{k,q}^{L_\alpha/2}(x,\, y)10^{\xi_{k,q}/20}} \sum_{l=0}^{L-1} \zeta_{k,q}^{l}(t) \exp\left(-j2\pi sd \sin\theta_{k,q,l}/\lambda_\omega\right) \delta(t - lT_c) \quad (3)$$

where α_c is a function of carrier frequency, antenna heights and antenna gains, which is assumed constant for all paths between a mobile set and a base station; $\theta_{k,q,l}$ is the direction of arrival (DoA) in BS q in the lth path for user k; λ_ω is signal wavelength; d is the distance between the antenna elements that should be defined as $d = 0.5\lambda$ in order to avoid the spatial aliasing; L is the total number of paths and is related to the delay spread; $\delta(.)$ is the Dirac delta function, and

$$\zeta_{k,q}^{l}(t) = \eta_{k,q}^{l}(t) e^{j\vartheta_{k,q}^{l}(t)} \quad (4)$$

where $\eta_{k,q}^{l}(t)$ and $\vartheta_{k,q}^{l}(t)$ denote the path gain and the path phase between MS k and BS q in the lth path, respectively [3].

Throughout our analysis, we will assume the following [3,4]

1. $\{\zeta_{k,q}^{l}(t)\}$s are constant, at least, during T_b time epochs (slow fading assumption), i.e., $\zeta_{k,q}^{l}(t) = \zeta_{k,q}^{l,n}$ where $nT_b \leq t \leq (n+1)T_b$.
2. $\{\eta_{k,q}^{l,n}\}$s mutually independent, and Nakagami distributed, with a probability density function given by

$$p_{\eta_{k,q}^{l,n}}(\eta) = \frac{2m_l^{m_l}\eta^{2m_l-1}}{\Omega_l^{m_l}\Gamma(m_l)} \exp\left(-\eta^2\frac{m_l}{\Omega_l}\right) U(\eta) \quad (5)$$

with the parameters

$$\Omega_l = \mathrm{E}\left[\eta_l^2\right] \quad (6)$$

$$m_l = \frac{\Omega_l^2}{\mathrm{E}\left[\left(\eta_l^2 - \Omega_l\right)^2\right]} \geq 0.5 \quad (7)$$

also in (5),

$$\Gamma(x) = \int_0^\infty \tau^{x-1} e^{-\tau} d\tau \quad (8)$$

is the gamma function [34]. The parameter m_l is the Nakagami severity of fading parameter (Nakagami-m fading parameter) of the lth resolvable path. It is well known that $m = 1$ corresponds to Rayleigh fading, $m = \infty$ corresponds to the non-fading condition, and $m = 0.5$ (one-sided Gaussian fading) corresponds to the worst case fading condition. Also, the Rician and lognormal distributions can be closely approximated by the Nakagami distribution with $m > 1$ [27,35–38]. On the other hand, the $\{\Omega_l\}$s are related to the channel's multipath intensity profile (MIP), which is typically a decreasing function of the delay. In this paper, we assume both the constant and exponentially decaying MIP distribution as follows.

$$\Omega_l = \Omega_0 e^{-\Delta l}, \quad \Delta \geq 0 \quad (9)$$

where Ω_0 is the average signal strength corresponding to the first incoming path and Δ reflects the rate at which the average fading strength decays.

3. $\{\vartheta_{k,q}^{l,n}\}$s are independent identically distributed (iid) random variables uniformly distributed in $[0, 2\pi)$.

Analytically, after combining, spreading and modulating the basic rate data streams, the reverse link transmitted low-pass equivalent resulting signal corresponding to user k in cell q, referred to the nominal carrier angular frequency $\omega_\circ$, is given by [4]

$$\tilde{s}_k(t) = \sqrt{P\lambda_k}\frac{\min_{q\in\Theta_k}\left\{d_{k,q}^{L_\alpha/2}(x,y)10^{\xi_{k,q}/20}\right\}}{\sqrt{\chi_{F_{kq}}}}b_k(t-\tau_k)c_k(t-\tau_k)e^{j\phi_k} \tag{10}$$

where $P = E_b/T_b$ represents the nominal received signal power of all users in the presence of perfect power control (PPC), where E_b is the energy per bit for all users. The variable λ_k is PCE for user k, which is assumed to follow a log-normal distribution and thus can be written as $\lambda_k = 10^{\upsilon_k/10}$, where υ_k is a Gaussian random variable with mean m_υ and variance σ_υ^2 [3,10]. Also, the variable Θ_k defines the set of the nearest BSs to user k; $c_k(t)$ is the pseudo noise (PN) chips of user k with a chip period of T_c; $b_k(t)$ is the information bit sequence of user k with a bit period of $T_b = GT_c$ where G is processing gain; τ_k denotes the timing offset of user k which is assumed to be uniformly distributed in $[0, T_b)$ and ϕ_k is the phase angle of the k user's carrier frequency which is assumed to be uniformly distributed in $[0, 2\pi)$.

The low-pass equivalent signal received from all users in sensor s of the BS0 can be written as [29,34]

$$\begin{aligned} r_{0,s}(t) &= \sum_k \tilde{s}_k(t)^* h_{k,0,s}(t) + n(t) \\ &= \sum_k \varepsilon_k\sqrt{P\lambda_k\Gamma_k(x,y)}\sum_{l=0}^{L-1}\zeta_{k,0}^l(t)b_k(t-lT_c-\tau_{k,0,l})c_k(t-lT_c-\tau_{k,0,l}) \\ &\quad\times\exp(-jsk_d\sin\theta_{k,0,l}) + n(t) \end{aligned} \tag{11}$$

where $k_d = 2\pi d/\lambda_\omega$ and $\tau_{k,0,l}$ denotes the timing offset between user k and BS0 in the lth path. Let $b_k(t) = \sum_i b_k(i)g(t-iT_b)$, where $g(t)$ is the basic pulse shape and $b_k \in \{-1, 1\}$ is the binary data of user k with $E[b_k(i)] = 0$ and $E[b_k(i)b_k(i')] = \delta_{ii'}$, $\delta_{ii'} = 1$ for $i = i'$ and $\delta_{ii'} = 0$ otherwise, and $E[b_k(i)b_{k'}(i')] = 0$ for $k \neq k'$. The voice activity ε_k for user k is modeled as a Bernoulli (ρ) random variable with $\Pr(\varepsilon_k = 1) = \rho$, and $\Pr(\varepsilon_k = 0) = 1-\rho$. Also $n(t)$ is an additive white Gaussian noise (AWGN) process with a two-sided power spectral density (PSD) of $N_0/2$ and

$$\Gamma_k(x,y) = \begin{cases} 1; & k \in S_{\mathrm{BS0}} \\ \dfrac{\min_{\substack{q\in\Theta_k \\ q\neq 0}}\left\{d_{k,q}^{L\alpha}(x,y)10^{\xi_{k,q}/10}\right\}}{d_{k,0}^{L\alpha}(x,y)10^{\xi_{k,0}/10}}\times\dfrac{\chi_{F_{k0}}}{\chi_{F_{kq}}}; & k \in S_{\overline{\mathrm{BS0}}} \\ \dfrac{\min_{q\in\Theta_k}\left\{d_{k,q}^{L\alpha}(x,y)10^{\xi_{k,q}/10}\right\}}{d_{k,0}^{L\alpha}(x,y)10^{\xi_{k,0}/10}}\times\dfrac{\chi_{F_{k0}}}{\chi_{F_{kq}}}; & k \in S_1 \end{cases} \tag{12}$$

where $\xi_{k,0}$ is a random variable modeling the shadowing between user k and BS0 with mean 0 and variance of σ_s^2 and $d_{k,0}(x,y)$ is the distance between user k and BS0 (see Fig. 2). In addition, according to Fig. 3, S_{BS0} denoting the set of users in S_0 that are connected to BS0 and $S_{\overline{\mathrm{BS0}}}$ is the set of users that are in central cell but not connected to BS0 [2].

Now, the received signal in sensor s of BS0 for user i (desired user) is given by [10]

$$r'_{i,0,s}(t) = \sqrt{P\lambda_i}\sum_{l=0}^{L-1}\zeta_{i,0}^{l}(t)b_i(t-lT_c-\tau_{i,0,l})c_i(t-lT_c-\tau_{i,0,l})\exp(-jsk_d\sin\theta_{i,0,l}) + I_{i,0,s}(t)+n(t) \tag{13}$$

where $I_{i,0,s}(t)$ is the total interference (intracell and intercell interferences) for user i in sensor s of BS0 and can be shown to be

$$I_{i,0,s}(t) = \sum_{\substack{k\\k\neq i}}\sum_{l=0}^{L-1}\zeta_{k,0}^{l}(t)\varepsilon_k\sqrt{P\lambda_k\Gamma_k(x,y)}b_k(t-lT_c-\tau_{k,0,l})c_k(t-lT_c-\tau_{k,0,l}) \times\exp(-jsk_d\sin\theta_{k,0,l}) \tag{14}$$

3 Rake Receiver Performance Analysis

The RAKE receiver structure in the DS-CDMA cellular system is shown in Fig. 1. The received signal is spatially processed by a CG beamforming circuit, one for each resolvable path (L_r beamformers, where $L_r \leq L$). The resultant signal is then passed on to a set of parallel matched filters (MFs), on a finger-by-finger basis. Also, the output signals from the L_r MFs are combined according to the conventional MRC principle and then are fed into the decision circuit for the desired user.

3.1 Conjugate Gradient Adaptive Beamforming

It is well known that an array of N weights has $N-1$ degree of freedom for adaptive beamforming [29,34]. This means that with an array of N weights, one can generate $N-1$ pattern nulls and a beam maximum in desired directions. From Sect. 2, it is clear that the number of users in the system is MK and the number of interference signals is $LMK-1$. To null all of these interference signals, one would have to have LMK weights, which is not practical. So, we focus only on the L paths of the desired user (inter-path interference (IPI)). Thus, the minimum number of the antenna array weights is L where, typically, L varies from 2 to 10.

In this paper, we use the CG adaptive beamforming (CGBF) algorithm that is based on orthogonal principle [29–32]. On this basis, a set of vectors $\mathbf{w}_i$ is to be selected such that they are $\mathbf{A}$-orthogonal, i.e., $\langle \mathbf{A}\mathbf{w}_i, \mathbf{A}\mathbf{w}_j\rangle = 0$ for $i \neq j$. The optimum weights in the jth branch ($1 \leq j \leq L_r$) at time n for user i in BS0 are obtained by minimizing [26,29]

$$\left\|\mathbf{x}_{i,0}^{(j)}(n)\right\|^2 = \mathbf{x}_{i,0}^{H(j)}(n)\mathbf{x}_{i,0}^{(j)}(n) \tag{15}$$

with

$$\mathbf{x}_{i,0}^{(j)}(n) = \mathbf{A}_0\mathbf{w}_{i,0}^{(j)}(n) - \mathbf{y}_{i,0}^{(j)} \tag{16}$$

where $\mathbf{A}_0$ is the $N\times N$ signal matrix in BS0 and using (11) is defined as follows.

$$\mathbf{A}_0 = \begin{bmatrix} r_{0,-(N-1)} & \cdots & r_{0,0} \\ \cdot & \cdot & \cdot \\ r_{0,0} & \cdots & r_{0,+(N-1)} \end{bmatrix} \tag{17}$$

Also in (16),

$$\mathbf{y}_{i,0}^{(j)} = \left[e^{-j(N-1)\theta_{i,0,j}/2} \ \ldots\ 1 \ldots e^{+j(N-1)\theta_{i,0,j}/2}\right]^T \tag{18}$$

and

$$\mathbf{w}_{i,0}^{(j)}(n) = \left[w_{i,0,0}^{(j)}(n) w_{i,0,1}^{(j)}(n) \quad \ldots \quad w_{i,0,N-1}^{(j)}(n)\right]^T \tag{19}$$

are the excitation and weight vectors ($N \times 1$) in the jth branch of BS0 for user i, respectively.

It should be mentioned that CG algorithm has two main characteristics [29,30]:

1. This algorithm can produce a solution of the matrix equation very efficiently and converge in a finite number of iterations (the number of beamformer weights).
2. In this algorithm, the convergence is guaranteed for any possible condition of the signal matrix, according to (17).

According to the algorithm of CG, the updated value of the weight vector for user i in the jth branch of BS0 at time $n+1$ is computed by using the simple recursive relation [29,30]:

$$\mathbf{w}_{i,0}^{(j)}(n+1) = \mathbf{w}_{i,0}^{(j)}(n) + \kappa_{i,0}^{(j)}(n)\boldsymbol{\beta}_{i,0}^{(j)}(n) \tag{20}$$

where

$$\begin{aligned}
\kappa_{i,0}^{(j)}(n) &= \left\|\mathbf{A}_0^H \mathbf{x}_{i,0}^{(j)}(n)\right\|^2 \Big/ \left\|\mathbf{A}_0 \boldsymbol{\beta}_{i,0}^{(j)}(n)\right\|^2 \\
\mathbf{x}_{i,0}^{(j)}(n+1) &= \mathbf{x}_{i,0}^{(j)}(n) + \kappa_{i,0}^{(j)}(n)\boldsymbol{\beta}_{i,0}^{(j)}(n) \\
\boldsymbol{\beta}_{i,0}^{(j)}(0) &= -\mathbf{A}_0^H \mathbf{x}_{i,0}^{(j)}(0) \\
\boldsymbol{\beta}_{i,0}^{(j)}(n+1) &= \mathbf{A}_0^H \mathbf{x}_{i,0}^{(j)}(n+1) + \eta_{i,0}^{(j)}(n)\boldsymbol{\beta}_{i,0}^{(j)}(n) \\
\eta_{i,0}^{(j)}(n) &= \left\|\mathbf{A}_0^H \mathbf{x}_{i,0}^{(j)}(n+1)\right\|^2 \Big/ \left\|\mathbf{A}_0^H \mathbf{x}_{i,0}^{(j)}(n)\right\|^2
\end{aligned} \tag{21}$$

The output signal from the jth CG beamformer can be written as [29]

$$y_{i,0}^{(j)}(t) = \sqrt{P\lambda_i}\,\zeta_{i,0}^{j}(t) b_i(t - jT_c - \tau_{i,0,j}) c_i(t - jT_c - \tau_{i,0,j}) + I_{i,0}^{(j)}(t) + n^{(j)}(t) \tag{22}$$

where $n^{(j)}(t)$ is a zero mean Gaussian noise of variance σ_n^2 and $I_{i,0}^{(j)}(t)$, the MAI, is defined as

$$\begin{aligned}
I_{i,0}^{(j)}(t) = \sum_{\substack{k \\ k\neq i}} \sum_{l=0}^{L-1} & \zeta_{k,0}^{l}(t)\varepsilon_k \sqrt{P\lambda_k \Gamma_k(x,y)}\, g_{i,0}^{(j)}\left(\theta_{k,0,l}\right) b_k(t - lT_c - \tau_{k,0,l}) \\
& \times c_k(t - lT_c - \tau_{k,0,l})
\end{aligned} \tag{23}$$

where

$$g_{i,0}^{(j)}(\theta) = \left[e^{-j(N-1)\theta/2} \ldots 1 \ldots e^{+j(N-1)\theta/2}\right] \times \mathbf{w}_{i,0}^{(j)} \tag{24}$$

is the magnitude response of the jth beamformer at BS0 for user i toward the direction of arrival θ and $\mathbf{w}_{i,0}^{(j)}$ is the jth beamformer's weight vector at BS0 for user i [29].

3.2 Matched Filter Stage

Using beamforming will only cancel out the inter-path interference for the desired user and will reduce the MAI from the users whose signals arrive at different angles from the desired user signal (out-beam interference). Now, in the second stage of the RAKE receiver, the output signal from the jth beamformer is directly passes on to a filter matched to the desired user's signature sequence. The jth MF output corresponding to the nth bit is [29]:

$$z_{i,0}^{(j)}(n) = \sqrt{P\lambda_i}\zeta_{i,0}^{j,n} b_i(n) + I_{i,0}^{\prime(j)}(n) + n^{\prime(j)}(n) \tag{25}$$

where

$$I_{i,0}^{\prime(j)}(n) = \frac{1}{T_b} \int_{(n-1)T_b+\tau_{i,0,j}}^{nT_b+\tau_{i,0,j}} I_{i,0}^{(j)}(t) c_i(t - jT_c - \tau_{i,0,j}) dt \tag{26}$$

and

$$n^{\prime(j)}(n) = \frac{1}{T_b} \int_{(n-1)T_b+\tau_{i,0,j}}^{nT_b+\tau_{i,0,j}} n^{(j)}(t) c_i(t - jT_c - \tau_{i,0,j}) dt \tag{27}$$

If we assume that the paths' delays from all users are less than the bit duration ($\tau_{k,q,l} < T_b$) for all users' signals on all paths, the nth bit MAI at the output of the jth MF can be expressed as [29]

$$I_{i,0}^{\prime(j)}(n) = \sum_{\substack{k \\ k\neq i}} \sum_{l=0}^{L-1} \zeta_{k,0}^{l,n} \varepsilon_k \sqrt{P\lambda_k \Gamma_k(x,y)} g_{i,0}^{(j)}(\theta_{k,0,l}) b_k(n) R_{i,k}(\tau_{i,0,j} - \tau_{k,0,l} + (j-l)T_c) \tag{28}$$

where the autocorrelation function $R_{i,k}(\tau)$ is defined as follows [29,39].

$$R_{i,k}(\tau) = \frac{1}{T_b} \int_{T_b} c_i(t) c_k(t+\tau) dt \tag{29}$$

If all users' delays are multiples of the chip period (T_c), then

$$R_{i,k}(\tau) = \frac{1}{G} \sum_{l_1=0}^{G-1} \sum_{l_2=0}^{G-1} c_i(l_1) c_k(l_2) R_c(\tau - (l_1 - l_2)T_c) \tag{30}$$

where the autocorrelation function $R_c(\tau)$ is:

$$R_c(\tau) = \frac{1}{T_b} \int_{T_b} c(t) c(t+\tau) dt \tag{31}$$

In the case of a maximal-length sequence (m-sequence) and for $0 \le \tau \le T_b$, we have [39]:

$$R_c(\tau) = \begin{cases} 1 - \frac{|\tau|}{T_c}(1 + 1/G); & |\tau| \le T_c \\ -1/G; & |\tau| \ge T_c \end{cases} \tag{32}$$

3.3 Maximal Ratio Combining Stage

Diversity combining has been considered as an efficient way to combat multipath fading because the combined SINR is increased compared with the SINR of each diversity branch. The optimum combiner is the MRC whose SINR is the sum of the SINRs of each individual diversity branch [39,40].

After the finger-MF, the fingers' signals are combined according to the MRC principle in the third stage of the RAKE receiver. In this paper, we use the conventional MRC that the signal of user i in the jth branch of BS0 is combined using multiplying by the complex conjugate of $\zeta_{i,0}^{j,n}$. Accordingly, the sample at the output of the conventional MRC of the RAKE receiver for the desired user in the central cell corresponding to the nth bit in the time interval $nT_b \leq t \leq (n+1)T_b$ can be expressed as follows [3].

$$\mathrm{Z}_{i,0,n} = (\mathrm{Z}_{i,0,n})_u + (\mathrm{Z}_{i,0,n})_{S_{\mathrm{BS0}}} + (\mathrm{Z}_{i,0,n})_{S_{\overline{\mathrm{BS0}}}} + (\mathrm{Z}_{i,0,n})_{S_1} + (\mathrm{Z}_{i,0,n})_{N_{th}} \tag{33}$$

As it can be observed, the sample $\mathrm{Z}_{i,0,n}$ at the output of the MRC is separated into a desired signal component and four noise components. The first noise component is due to multiple access intracell interference from the users in S_{BS0}. The second and third components are due to multiple access intercell interference from the users in $S_{\overline{\mathrm{BS0}}}$ and S_1, respectively, and the fourth component is due to AWGN.

Thus, using (25), the desired signal component in the jth output of the MRC corresponding to the nth bit for user i at BS0 can be expressed as follows.

$$(\mathrm{Z}_{i,0,n})_u^j = \sqrt{P\lambda_i} b_i(n) \left|\zeta_{i,0}^{j,n}\right|^2 \tag{34}$$

Now using (4), (34) can be rewritten as follows.

$$(\mathrm{Z}_{i,0,n})_u^j = \sqrt{P\lambda_i} b_i(n) \left(\eta_{i,0}^{j,n}\right)^2 \tag{35}$$

Accordingly, the desired signal component in the output of the RAKE receiver for user i at BS0 can be written as follows.

$$U_s \triangleq (\mathrm{Z}_{i,0,n})_u = \sum_{j=1}^{L_r} (\mathrm{Z}_{i,0,n})_u^j = \sqrt{P\lambda_i} b_i(n) \sum_{j=1}^{L_r} \left(\eta_{i,0}^{j,n}\right)^2 \tag{36}$$

On the other hand, the interference signal component (intracell and intercell interferences) in the jth output of the MRC for the desired user at BS0 can be written as follows.

$$\widehat{I}_{i,0}^{j}(n) = \sum_{\substack{k \\ k \neq i}} \varepsilon_k \sqrt{P\lambda_k \Gamma_k(x,y)} b_k(n) \sum_{l=0}^{L-1} \eta_{i,0}^{j,n} \eta_{k,0}^{l,n} g_{i,0}^{(j)}(\theta_{k,0,l}) R_{i,k}\left(\tau_{i,0,j} - \tau_{k,0,l} + (j-l)T_c\right) \tag{37}$$

4 Error Probability Analysis

4.1 Gaussian Assumption

In the performance analysis of DS-CDMA cellular systems, the interference terms are usually assumed to be Gaussian distributed. The use of the Gaussian assumption in BER calculations is very common. A number of approaches are available to improve the accuracy of the

Gaussian approximation [27,41]. In this paper, we employ the Gaussian approximation and model the MAI as AWGN process with variance equal to the MAI. It is well known that, conditioned on $\eta_{i,q}^{j,n}$, the variance of both intracell and intercell interferences in the jth branch can be written as

$$\begin{aligned}\sigma_{S_x,j}^2 &= \mathrm{E}\left[\left(\widetilde{I}_{i,0}^{j}(n)\right)^2\right] \\ &= \mathrm{E}\left[\left(\sum_{\substack{k\in S_x\\ k\neq i}} \varepsilon_k\sqrt{P\lambda_k\Gamma_k(x,y)}b_k(n)\sum_{l=0}^{L-1}\eta_{i,0}^{j,n}\eta_{k,0}^{l,n}g_{i,0}^{(j)}\left(\theta_{k,0,l}\right)R_{i,k}\right.\right. \\ &\qquad \left.\left.\times\left(\tau_{i,0,j}-\tau_{k,0,l}+(j-l)T_c\right)\right)^2\right] \\ &= P\left(\eta_{i,0}^{j,n}\right)^2\sum_{\substack{k\in S_x\\ k\neq i}}\mathrm{E}(\varepsilon_k)\mathrm{E}(\lambda_k)\mathrm{E}(\Gamma_k(x,y))\varpi_k\sum_{l=0}^{L-1}\mathrm{E}\left(\left(\eta_{k,0}^{l,n}\right)^2\right)\end{aligned} \tag{38}$$

where $S_x \in \{S_{\mathrm{BS0}}, S_{\overline{\mathrm{BS0}}}, S_1\}$ and ϖ_k is the average cross-correlation and CG adaptive beamforming over all paths ($0 \le l \le L-1$) and all branches ($1 \le j \le L_r$) for user k. Also, in (38), we have $\mathrm{E}(\varepsilon_k) = \rho$ and $\mathrm{E}[\lambda_k] = e^{\beta m_\upsilon + \beta^2\sigma_\upsilon^2/2}$, where $\beta = \ln 10/10$ [4,10]. Accordingly, using (6), (38) can be rewritten as follows.

$$\sigma_{S_x,j}^2 = P\left(\eta_{i,0}^{j,n}\right)^2\rho e^{\beta m_\upsilon+\beta^2\sigma_\upsilon^2/2}\sum_{l=0}^{L-1}\Omega_l\sum_{\substack{k\in S_x\\ k\neq i}}\varpi_k\mathrm{E}(\Gamma_k(x,y)) \tag{39}$$

For simplicity, we assume that $\varpi_k = \varpi_\circ$ for all users. Now using (9), (39) can be rewritten as

$$\sigma_{S_x,j}^2 = P\left(\eta_{i,0}^{j,n}\right)^2\rho e^{\beta m_\upsilon+\beta^2\sigma_\upsilon^2/2}\varpi_\circ\Omega_\circ q(L,\Delta)\sum_{\substack{k\in S_x\\ k\neq i}}\mathrm{E}(\Gamma_k(x,y)) \tag{40}$$

where $q(L,\Delta) = \sum_{l=0}^{L-1} e^{-\Delta l} = \frac{1-e^{-\Delta L}}{1-e^{-\Delta}}$.

Using (12) and considering statistically independent random variables, we define [4]

$$\omega_{s_x} = \mathrm{E}\left[\frac{1}{K}\sum_{k\in s_x}\Gamma_k(x,y)\right] \tag{41}$$

where ω_{S_x} for $S_x \in \{S_{\mathrm{BS0}}, S_{\overline{\mathrm{BS0}}}, S_1\}$ is shown in Appendix A. Tables 1 and 2 provide the values obtained for $\omega_{S_{\overline{\mathrm{BS0}}}}$ and ω_{S_1} for different values of path-loss exponent L_α, variance of the lognormal shadowing σ_s^2, and number of BSs in the selection process Q_c. We have considered a cellular layout with 81 cells, corresponding to the central cell plus the four closest rings of cells surrounding it as Fig. 3a. As shown in Table 3 and in agreement with the results presented by Femenias and Carrasco [4], our results show that the average intercell interference, which is proportional to $\omega_{S_{\overline{\mathrm{BS0}}}} + \omega_{S_1}$, increases as the path-loss exponent L_α decreases due to the decrement of the average attenuation. In addition, as the variance of the lognormal shadowing σ_s^2 increases, the influence of distant users becomes dominant, and

Table 1 $\omega_{S_{\overline{\text{BS0}}}}$ for different values of system parameters

L_α	Q_c	$\sigma_s^2 = 2$ dB	$\sigma_s^2 = 4$ dB	$\sigma_s^2 = 6$ dB	$\sigma_s^2 = 8$ dB
3	4	0.7293	0.6837	0.6398	0.5995
	9	0.8636	0.8118	0.7742	0.7332
	25	1.0027	0.9243	0.8597	0.8029
4	4	0.5332	0.5192	0.4872	0.4329
	9	0.6121	0.5821	0.5512	0.5011
	25	0.6798	0.6503	0.6138	0.5629
5	4	0.4781	0.4693	0.4496	0.4009
	9	0.5491	0.5239	0.4893	0.4611
	25	0.5529	0.5379	0.5174	0.4994

Table 2 ω_{S_1} for different values of system parameters

L_α	Q_c	$\sigma_s^2 = 2$ dB	$\sigma_s^2 = 4$ dB	$\sigma_s^2 = 6$ dB	$\sigma_s^2 = 8$ dB
3	4	0.6673	0.8932	1.3471	2.1208
	9	0.4129	0.5193	0.8531	1.6439
	25	0.1009	0.2113	0.3728	0.6411
4	4	0.2019	0.5112	1.1281	1.4386
	9	0.1013	0.1923	0.2887	0.3983
	25	0.0071	0.0903	0.1797	0.2520
5	4	0.1094	0.2117	0.7631	0.9442
	9	0.0116	0.0915	0.1909	0.2866
	25	0.0017	0.0302	0.0898	0.1292

the average intercell interference increases. Furthermore, as expected, the average intercell interference decreases with an increase in Q_c.

Accordingly, we can rewrite (40) as follows.

$$\sigma_{S_x,j}^2 = P\left(\eta_{i,0}^{j,n}\right)^2 \rho e^{\beta m_\upsilon + \beta^2\sigma_\upsilon^2/2}\varpi_\circ\Omega_\circ q(L,\Delta)K\omega_{s_x} \tag{42}$$

Also, according to (33), the variance of the Gaussian noise term in the jth branch of BS0, conditioned on $\eta_{i,0}^{j,n}$, is given as

$$\sigma_{n,j}^2 = \frac{N_0}{2T_b}\left(\eta_{i,0}^{j,n}\right)^2 \tag{43}$$

Now, using (42) and (43), the variances of MAI and Gaussian noise term at the output of the RAKE receiver can be written as follows.

$$\sigma_{S_x}^2 = \left(P\rho e^{\beta m_\upsilon + \beta^2\sigma_\upsilon^2/2}\varpi_\circ\Omega_\circ q(L,\Delta)K\omega_{s_x}\right) \times \sum_{j=1}^{L_r}\left(\eta_{i,0}^{j,n}\right)^2 \tag{44}$$

$$\sigma_n^2 = \frac{N_0}{2T_b}\sum_{j=1}^{L_r}\left(\eta_{i,0}^{j,n}\right)^2 \tag{45}$$

Table 3 $\omega_{S_{\overline{\text{BS0}}}} + \omega_{S_1}$ for different values of system parameters

L_α	Q_c	$\sigma_s^2 = 2$ dB	$\sigma_s^2 = 4$ dB	$\sigma_s^2 = 6$ dB	$\sigma_s^2 = 8$ dB
3	4	1.3966	1.5769	1.9869	2.7203
	9	1.2765	1.3311	1.6273	2.3771
	25	1.1036	1.1356	1.2325	1.4440
4	4	0.7351	1.0304	1.6153	1.8715
	9	0.7134	0.7744	0.8399	0.8994
	25	0.6869	0.7406	0.7935	0.8149
5	4	0.5875	0.6810	1.2127	1.3451
	9	0.5607	0.6154	0.6802	0.7477
	25	0.5546	0.5681	0.6072	0.6286

Thus using (33), (44), and (45), the variance of the total interference can be written as

$$\begin{aligned}\sigma_T^2 &= \sigma_{S_{\text{BS0}}}^2 + \sigma_{S_{\overline{\text{BS0}}}}^2 + \sigma_{S_1}^2 + \sigma_n^2 \\ &= \left(P\rho e^{\beta m_\upsilon + \beta^2\sigma_\upsilon^2/2}\varpi_\circ\Omega_\circ q(L,\Delta)K\left(\omega_{S_{\text{BS0}}} + \omega_{S_{\overline{\text{BS0}}}} + \omega_{S_1}\right) + \frac{N_0}{2T_b}\right) \times \sum_{j=1}^{L_r}\left(\eta_{i,0}^{j,n}\right)^2\end{aligned} \tag{46}$$

where using Appendix A, $\omega_{S_{\text{BS0}}} = 1$.

Now using (36), the power of the desired signal at the output of the RAKE receiver can be written as

$$U_s^2 = P\lambda_i\left(\sum_{j=1}^{L_r}\left(\eta_{i,0}^{j,n}\right)^2\right)^2 = Pe^{\beta\upsilon_i}\left(\sum_{j=1}^{L_r}\left(\eta_{i,0}^{j,n}\right)^2\right)^2 \tag{47}$$

Accordingly, the received SINR at the output of the RAKE receiver, U_s^2/σ_T^2, may be written in compact form as $\sigma_0 S$, where

$$S = Pe^{\beta\upsilon_i}\sum_{j=1}^{L_r}\left(\eta_{i,0}^{j,n}\right)^2 \tag{48}$$

$$\sigma_0 = \left\{P\rho e^{\beta m_\upsilon + \beta^2\sigma_\upsilon^2/2}\varpi_\circ\Omega_\circ q(L,\Delta)K\left(1 + \omega_{S_{\overline{\text{BS0}}}} + \omega_{S_1}\right) + \frac{N_0}{2T_b}\right\}^{-1} \tag{49}$$

4.2 PDF of SINR

The SINR at the output of the RAKE receiver in BS0 is a function of the sum of the squares of signal strengths $\eta_{i,0}^{j,n}$, given by [27]

$$\gamma = \sum_{j=1}^{L_r}\left(\eta_{i,0}^{j,n}\right)^2 \tag{50}$$

The pdf of γ can be shown to be given by

$$p(\gamma) = \frac{1}{\pi} \int_0^{\infty} \frac{\cos\left[\sum_{l=0}^{L-1} m_l \tan^{-1}(t/\lambda_l) - t\gamma\right]}{\prod_{l=0}^{L-1}\left[1 + \left(\frac{t}{\lambda_l}\right)^2\right]^{m_l/2}} dt \tag{51}$$

where $\lambda_l = m_l/\Omega_l, l = 0, 1, \ldots, L-1$ [27,35].

4.3 BER Analysis

For coherent demodulation in the presence of AWGN, the probability of error conditioned on the instantaneous SINR can be written as [27]

$$P_e(S) = \frac{\Gamma\left(\frac{1}{2}, \sigma_\circ S\right)}{2\sqrt{\pi}} \tag{52}$$

where

$$\Gamma(b, x) = \int_x^{\infty} y^{b-1} e^{-y} dy \tag{53}$$

is the incomplete gamma function [34].

Accordingly, we have

$$\bar{P}_e = \int_0^{\infty} P_e(S) p(S) dS \tag{54}$$

The results for identical and integer of the Nakagami fading parameters in the different paths are available in the literature. Using [27] and for the general case of non-integer and non-identical fading parameters in the diversity branches, we can rewrite (54) as follows.

$$\begin{aligned}\bar{P}_e &= \int_0^{\infty} P_e(S) p(S) dS = \frac{1}{2\pi\sqrt{\pi}} \int_0^{\infty}\int_0^{\infty} \Gamma\left(\frac{1}{2}, \sigma_\circ S\right) \frac{\cos\left[\sum_{l=0}^{L-1} m_l \tan^{-1}(t/\lambda_l) - t\gamma\right]}{\prod_{l=0}^{L-1}\left[1+\left(\frac{t}{\lambda_l}\right)^2\right]^{m_l/2}} dt dS \\ &= \frac{1}{2\pi} \int_0^{\infty} \frac{1}{\prod_{l=0}^{L-1}\left[1+\left(\frac{t}{\lambda_l}\right)^2\right]^{m_l/2}} \times \left\{ \cos\left[\sum_{l=0}^{L-1} m_l \tan^{-1}(t/\lambda_l) - t\gamma\right] . \frac{\sqrt{\sigma_\circ}\sin\left[\frac{1}{2}\tan^{-1}(t/\sigma_\circ)\right]}{\left(t^2+\sigma_\circ^2\right)^{1/4}} \right. \\ &\quad \left. + \sin\left[\sum_{l=0}^{L-1} m_l \tan^{-1}(t/\lambda_l) - t\gamma\right] . \left[1 - \frac{\sqrt{\sigma_\circ}\cos\left[\frac{1}{2}\tan^{-1}(t/\sigma_\circ)\right]}{\left(t^2+\sigma_\circ^2\right)^{1/4}}\right] \right\} \frac{dt}{t}\end{aligned} \tag{55}$$

where, now, $\lambda_l = \Omega_\circ m_l/\Omega_l$ [27].

5 Other Beamforming Methods

5.1 Constrained LMS Algorithm

Constrained LMS algorithm is a gradient based algorithm to minimize the total processor output power, based on the look direction constraint. The adaptive algorithm is designed to

adapt efficiently to the environment and is able to permanently preserve the desired frequency response in the look direction while minimizing the output power of the array. In [42–44], we used the CLMS algorithm in order to decrease the interference of DS-CDMA cellular systems in multipath fading channels. In this algorithm, unlike the CGBF algorithm, the number of weights and sensors are equal, i.e., $S = N$. Accordingly, by the CLMS algorithm, the desired users' signal in an arbitrary path is passed but the IPI is not canceled in other paths in each RAKE finger, while the IPI is removed in the CGBF algorithm.

Accordingly, using (13), the output of the array with the CLMS algorithm in the nth iteration in the jth branch for user i in BS0 is given by [42–46]

$$y_{i,0}^{(j)}(n) = \mathbf{w}_{i,0}^{(j)}(n)^H \mathbf{r}'_{i,0}(n) \tag{56}$$

where $\mathbf{r}'_{i,0} = [r'_{i,0,0}\, r'_{i,0,1} \cdots r'_{i,0,N-1}]^T$.

The expected output power of the array in the nth iteration is given by

$$\begin{aligned} \mathrm{E}\left(\left|y_{i,0}^{(j)}(n)\right|^2\right) &= \mathrm{E}\left(y_{i,0}^{(j)}(n) y_{i,0}^{(j)}(n)^*\right) \\ &= \mathrm{E}\left(\mathbf{w}_{i,0}^{(j)}(n)^H \mathbf{r}'_{i,0}(n) \mathbf{r}'_{i,0}(n)^H \mathbf{w}_{i,0}^{(j)}(n)\right) = \mathbf{w}_{i,0}^{(j)}(n)^H \mathbf{R}_{r'r'} \mathbf{w}_{i,0}^{(j)}(n) \end{aligned} \tag{57}$$

where $\mathbf{R}_{r'r'}$ is the correlation matrix of the received vector $\mathbf{r}'_{i,0}(n)$.

A real-time CLMS algorithm for determining the optimal weight vector for user i in BS0 in the jth branch is [46]:

$$\begin{cases} \mathbf{w}_{i,0}^{(j)}(n+1) = \mathbf{w}_{i,0}^{(j)}(n) + \mu g\left(\mathbf{w}_{i,0}^{(j)}(n)\right) \\ \mathbf{w}_{i,0}^{(j)H} \mathbf{a}_{i,0}^{(j)}(\theta_{i,0,j}) = 1 \end{cases} \tag{58}$$

where

$$\mathbf{a}_{i,0}^{(j)}(\theta_{i,0,j}) = [1 \exp\left(-j2\pi d \sin\theta_{i,0,j}/\lambda\right) \ldots \exp\left(-j2\pi d(N-1)\sin\theta_{i,0,j}/\lambda\right)]^T \tag{59}$$

denotes spatial response of the array for user i in BS0 in the jth branch. Also, in (39), $\mathbf{w}_{i,0}^{(j)}(n+1)$ is the new weight computed at the $(n+1)$th iteration for user i in BS0 in the jth branch. Also, the variable scalar μ denotes a positive scalar (gradient step size) that controls the convergence characteristic of the algorithm, that is, how fast and how close the estimated weights approach the optimal weights, and $g(\mathbf{w}_{i,0}^{(j)}(n))$ denotes an unbiased estimate of the gradient of the power surface $(\mathbf{w}_{i,0}^{(j)}(n)^H \mathbf{R}_{r'r'} \mathbf{w}_{i,0}^{(j)}(n)$ which is the expected output power of the array) with respect to $\mathbf{w}_{i,0}^{(j)}(n)$ after the nth iteration. The algorithm is "constrained" because the weight vector satisfies the constraint at each iteration, that is $\mathbf{w}_{i,0}^{(j)H} \mathbf{a}_{i,0}^{(j)}(\theta_{i,0,j}) = 1$. We rewrite the CLMS algorithm as follows [46].

$$\mathbf{w}_{i,0}^{(j)}(n+1) = \boldsymbol{\psi}_{i,0}^{(j)}\left(\mathbf{w}_{i,0}^{(j)}(n) + \mu g\left(\mathbf{w}_{i,0}^{(j)}(n)\right)\right) + \frac{\mathbf{a}_{i,0}^{(j)}(\theta_{i,0,j})}{N} \tag{60}$$

where

$$\boldsymbol{\psi}_{i,0}^{(j)} = \mathbf{I} - \frac{\mathbf{a}_{i,0}^{(j)}(\theta_{i,0,j}) \mathbf{a}_{i,0}^{(j)}(\theta_{i,0,j})^H}{N} \tag{61}$$

The gradient of $\mathbf{w}_{i,0}^{(j)}(n)^H \mathbf{R}_{r'r'} \mathbf{w}_{i,0}^{(j)}(n)$ with respect to $\mathbf{w}_{i,0}^{(j)}(n)$ is given by [46]

$$g\left(\mathbf{w}_{i,0}^{(j)}(n)\right) \triangleq -\frac{\partial}{\partial \mathbf{w}_{i,0}^{(j)*}} \left(\mathbf{w}_{i,0}^{(j)}(n)^H \mathbf{R}_{r'r'} \mathbf{w}_{i,0}^{(j)}(n)\right) = -2\mathbf{R}_{r'r'} \mathbf{w}_{i,0}^{(j)}(n) \tag{62}$$

and its computation using this expression requires knowledge of $\mathbf{R}_{r'r'}$, which normally is not available in practice. For a standard LMS algorithm, an estimate of the gradient at each iteration is made by replacing $\mathbf{R}_{r'r'}$ by its noise sample $\mathbf{r'}_{i,0}(n+1)\mathbf{r'}_{i,0}(n+1)^H$ available at time instant $(n+1)$, leading to

$$g\left(\mathbf{w}_{i,0}^{(j)}(n)\right) = -2\mathbf{r'}_{i,0}(n+1) y_{i,0}^{(j)*}(n) \tag{63}$$

The CLMS is a fast convergence algorithm. However, it is drastically sensitive to the mismatch in the direction of arrival. Meanwhile, the weights estimated by the standard algorithm are sensitive to the signal power, requiring a lower step size in the presence of a strong signal for the algorithm to converge, which, in turn, leads to an increase in the convergence time due to a decrease in mis-adjustment error [46,47].

From the above discussion, we can conclude that the BER in the CGBF algorithm is less than that in the CLMS algorithm. In the simulation study, we will evaluate the average BER in a DS-CDMA receiver with the CGBF and CLMS algorithms.

5.2 Switched-Beam Technique

One simple alternative to the fully adaptive antenna is the switched-beam architecture in which the best beam is chosen from a number of fixed steered beams. Switched-beam systems are technologically the simplest and can be implemented by using a number of fixed, independent, or directional antennas [48]. We list the conditions of the SB technique for this paper as follows [49].

1. According to Fig. 4, beams coverage angle is 30° and overlap between consecutive beams is 20°. Thus each base station has 36 beams.
2. According to Fig. 5, each user can use one beam for each of its path to communicate with a base station at any time.

6 Simulation Results

In this section, we investigate the effects of the selection of system parameters on the BER performance of DS-CDMA cellular systems in Nakagami fading channels. Analytical and simulation results are also given for DS-CDMA cellular systems with different processing gains, number of resolvable paths, and Nakagami fading channel parameters showing the reductions in system capacity due to imperfect power control. Also, for simplicity, all paths are assumed to have the same fading parameter m (i.e., $m_l = m$ for $l = 0, 1, \ldots, L-1$). Accordingly, we assume a cellular layout with 81 cells ($M = 81$), corresponding to the central cell and the four closest rings of cells surrounding it as in Fig. 3a. We also assume a cell-selection process limited to $Q_c = 4$, 9, and 25 nearest base stations, frequency selective fading channels with $L = 10$ resolvable propagation paths; input data rate $T_b = 9.6$ Kbps; a mean of $m_\upsilon = 0$ for PCE; a processing gain of $G = 128$; signal to noise ratio, SNR $= E_b/N_0 = 10$ dB; a voice activity factor of $\rho = 0.3$; a lognormal shadow fading with a variance of $\sigma_s^2 = 4$ dB; the number of antenna weights and the number of antenna sensors in the CGBF algorithm

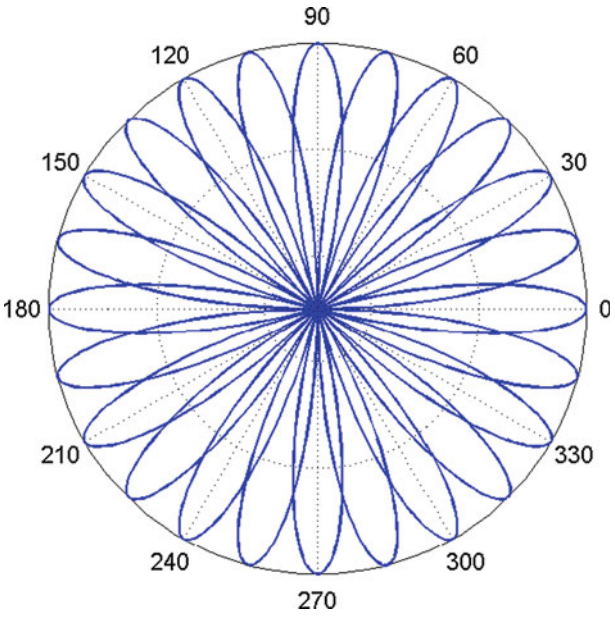

Fig. 4 Thirty-six beams in each base station with switched-beam technique

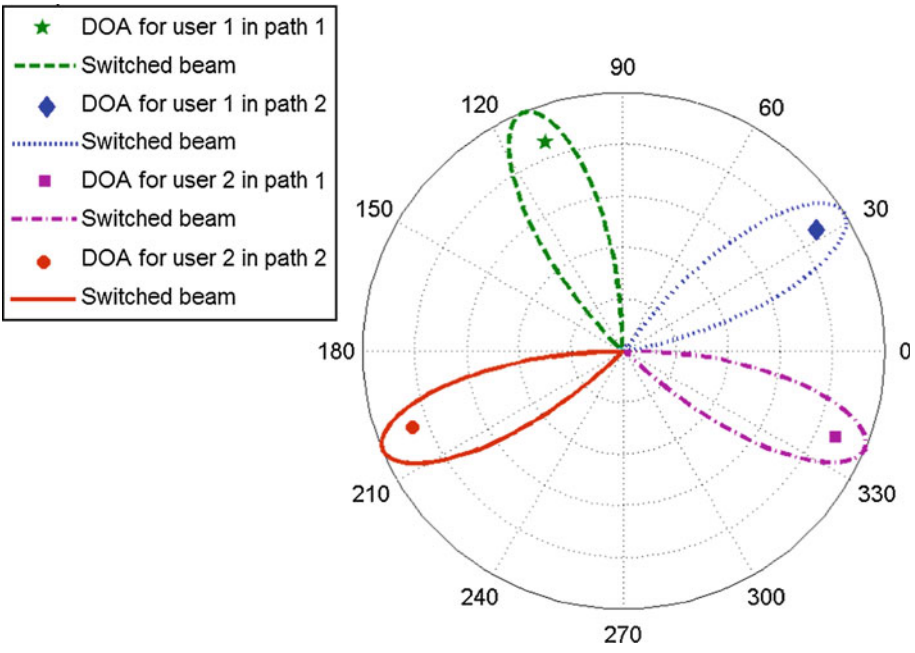

Fig. 5 Select of beam for two users in two paths with switched-beam technique

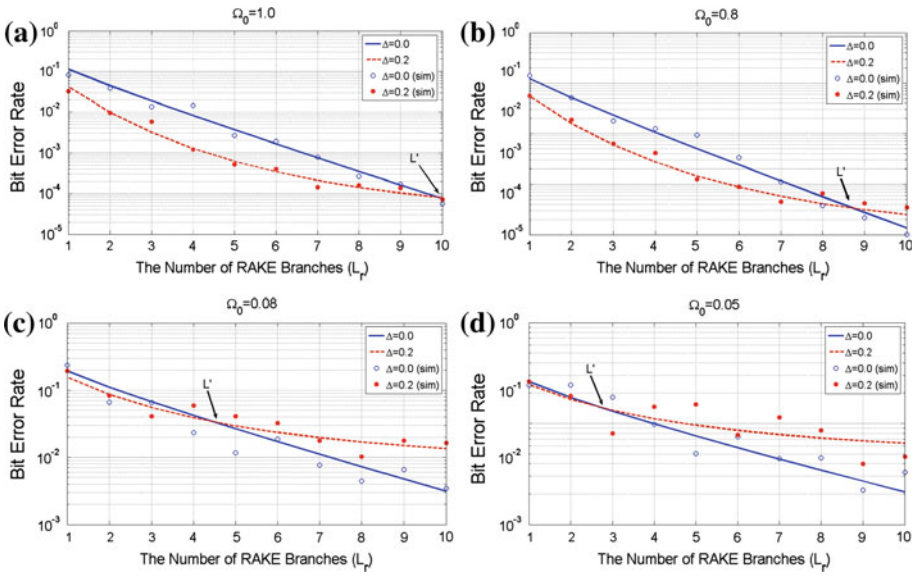

Fig. 6 Average BER versus the number of RAKE branches (L_r) for $\Delta = 0.0$, 0.2 and **a** $\Omega_0 = 1.0$ **b** $\Omega_0 = 0.8$ **c** $\Omega_0 = 0.08$ **d** $\Omega_0 = 0.05$ ($\sigma_\upsilon^2 = 0$ dB, $Q_c = 4$, $m = 1$, and $K = 40$)

$N = 3$ and $S = 5$, respectively; the number of antenna sensors in the CLMS algorithm $S = 3$; gradient step size in the CLMS algorithm $\mu = 0.005$; initial value for weight vectors in the CGBF and CLMS algorithms $\mathbf{w}(0) = \mathbf{0}$. The positions of the users and their temporal signatures are generated at random, but then kept fixed for the particular experiment.

The influence of the rate of average power decay (Δ) and average signal strength (Ω_0) on the average BER against the number of RAKE branches (L_r) for ($L_r \leq L$) is shown in Fig. 6. In this simulation, we assume the number of BSs in the cell-selection process $Q_c = 4$, the Nakagami fading parameter $m = 1$ for all paths, variance of PCE $\sigma_\upsilon^2 = 0$ dB (perfect power control), and there are $K = 40$ users randomly distributed in any cell with uniform distribution, as in Fig. 3a. It should be mentioned that in this simulation, we show the important conclusions of our paper. In agreement with the results presented by Efthymoglou et al. [27], we observe that for $L_r < L'$, better BER is achieved for $\Delta = 0.2$ than $\Delta = 0.0$, because the reduced MAI has a greater impact on system performance than the reduced signal power. However, the previous observation may be reversed if a space-time RAKE combiner with a greater number of fingers ($L' \leq L_r \leq L$) is used, as the sum of the signal powers of the different paths affects the BER more favorably than the increase of the MAI. Also, it can be seen that L' decreases as the average signal strength Ω_0 decreases. For example, for $\Omega_0 = 1.0$, 0.8, 0.08, and 0.05, we have $L' = 10$, 9, 5, and 3, respectively. Also, as expected, the average BER decreases as average signal strength (Ω_0) increases. In addition, as shown in Fig. 6, the analytical and simulated results are in acceptable agreement.

The influence of the number of rake fingers, the number of base stations in the cell-selection process, and PCE variance on the system performance are shown in Figs. 7 and 8. Accordingly, Fig. 7 shows the average BER for $K = 40$ users versus the number of rake fingers with the PCE variance and the number of base stations in the cell-selection process as parameters. In addition, Fig. 8 shows the average number of active users in any cell versus the PCE variance with the number of rake fingers and the number of BSs in the cell-selection

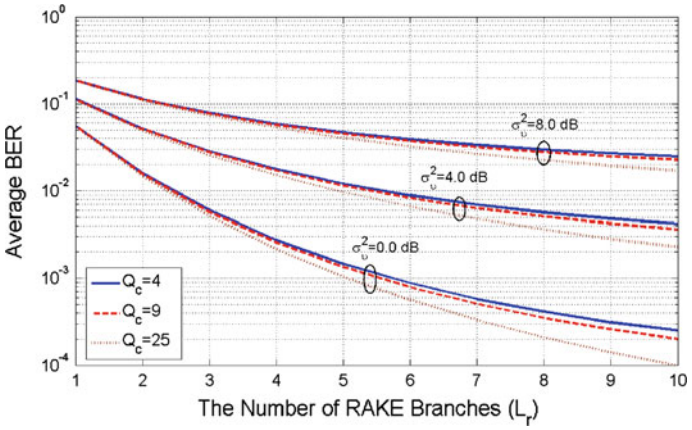

Fig. 7 Average BER versus the number of RAKE branches for different values of σ_υ^2 and Q_c

process as parameters for a required $p_b = 0.01$. In these simulations, we assume $m = 1$, the rate of average power decay $\Delta = 0.2$ and average signal strength $\Omega_0 = 0.8$ (therefore as Fig. 6b, we have $L' = 9$). As expected, the system performance improves along with an increase in L_r and Q_c, and degrades along with an increase in σ_υ^2. It can also be seen that the use of multipath diversity and cell-selection diversity exacerbates the degradation of the average BER performance of the system due to PCE, i.e., the use of selection-based diversity as well as multipath diversity increases the effects of PCE on the average BER. It can also be observed that for $L_r < L'$, the relative increased average BER degradation due to PCE, when using power control in conjunction with RAKE diversity combining and cell-selection diversity, does not directly translate into a relative increased capacity degradation of the system, while for $L' \leq L_r \leq L$, it can directly translate into a relative increased capacity degradation of the system. For example, as shown in Fig. 8, representing the capacity for $L_r < L'$ and a required $p_b = 10^{-2}$ versus the PCE variance with L_r and Q_c as parameters, a capacity decrease of approximately 12, 22, 37, and 64% can be observed when the PCE variance increases from 0 (perfect power control) to 1, 2, 4, and 8 dB, respectively, irrespective of the number of rake fingers for $L_r < L'$ and the number of BSs used in the selection-based diversity process. While for $L' \leq L_r \leq L$, a capacity decrease of approximately 14, 24, 42, and 71% can be observed.

The number of active users per cell for a specified BER is also an important design criterion. Figure 9 shows the average BER as a function of the number of active users per cell with processing gain (G_p) and Q_c as parameters. In this simulation, we assume $\Omega_0 = 0.8, m = 1, L_r = 5, \sigma_\upsilon^2 = 4\,\text{dB}$, and $\Delta = 0.2$. As expected, the average BER decreases as the processing gain increases. For example, with $Q_c = 25$, a 52% decrease in capacity can be seen for a required $p_b = 0.01$ when the processing gain decreases from $G_p = 256$ to $G_p = 128$. On the other hand, the number of BSs in the cell-selection process Q_c has a considerable effect on the number of active users per cell supported by the system. For example, for $G_p = 512$, a 61% decrease in capacity can be seen for a required $p_b = 0.002$ when the number of BSs in the cell-selection process decreases from $Q_c = 25$ to $Q_c = 9$. From this figure, we also observe that the processing gain has a greater effect on system performance for $Q_c = 25$ than that for $Q_c = 9$. In addition, when the number of active users per cell increases, better BER is achieved for $Q_c = 25$ than that for $Q_c = 9$.

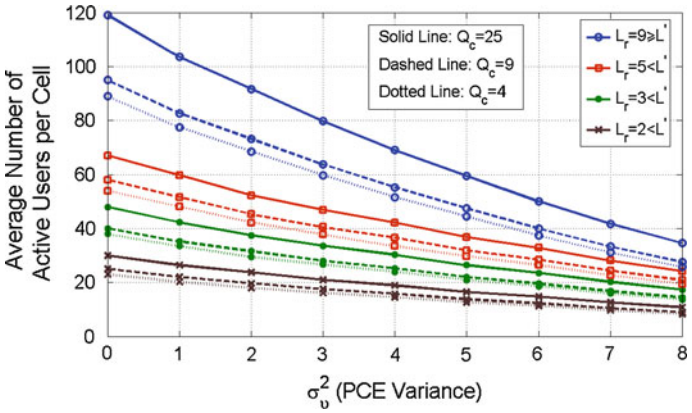

Fig. 8 Capacity (for a required $p_b = 0.01$) versus the PCE variance (σ_υ^2) for different values of L_r and Q_c

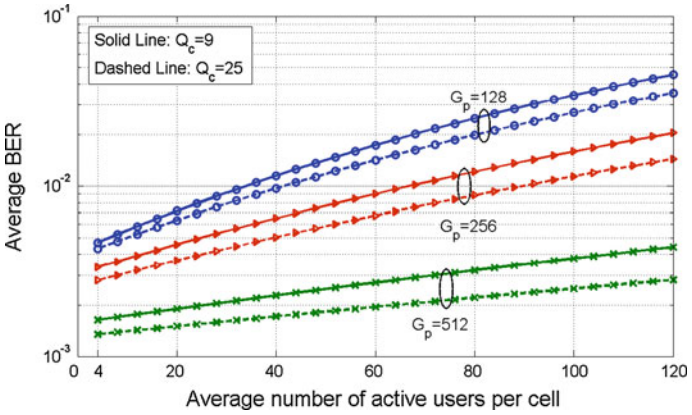

Fig. 9 Average BER versus the average number of active users per cell for different values of G_p and Q_c

The influence of the Nakagami-m fading parameter on the system capacity is illustrated in Fig. 10. In this figure p_b has been set to a fixed value of 0.01, $L_r = 5$, $\Omega_0 = 0.8$, and $\Delta = 0.2$. As expected, the number of active users increases as the Nakagami-m fading parameter increases. For example, for $\sigma_\upsilon^2 = 4$ dB and $Q_c = 25$, a 68% capacity increment can be seen when m increases from $m = 0.5$ to $m = 3$. As it can be seen in Fig. 9, Q_c is one of the parameters more strongly affecting the active users. For example, for $m = 3$ and $\sigma_\upsilon^2 = 4$ dB, the number of users allowed in any cell is $K = 49$ users for $Q_c = 9$, while for $Q_c = 25$ the number of users is $K = 59$ users. Also, it can be seen that the number of users allowed in the system for $\sigma_\upsilon^2 = 0$ dB is higher than that for $\sigma_\upsilon^2 = 4, 8$ dB. For example, for $Q_c = 25$ and $m = 4$, the number of users allowed in any cell is $K = 90$ users for $\sigma_\upsilon^2 = 0$ dB, while for $\sigma_\upsilon^2 = 4, 8$ dB the number of users is $K = 62$ users and $K = 37$ users, respectively.

Finally, Fig. 11 shows the average BER versus the number of active users in any cell for different receivers (one, two, and three-stage receivers), $L_r = 5$, $\Omega_0 = 0.8$, $\Delta = 0.2$, $\sigma_\upsilon^2 = 4$ dB, $m = 1$, and $Q_c = 9$. In this simulation, the three-stage RAKE receiver uses the CGBF, CLMS, or SB methods in the first stage. This figure shows that the number of users for a fixed BER in one-stage receiver (MF only) is lower than two-stage RAKE receiver. For example,

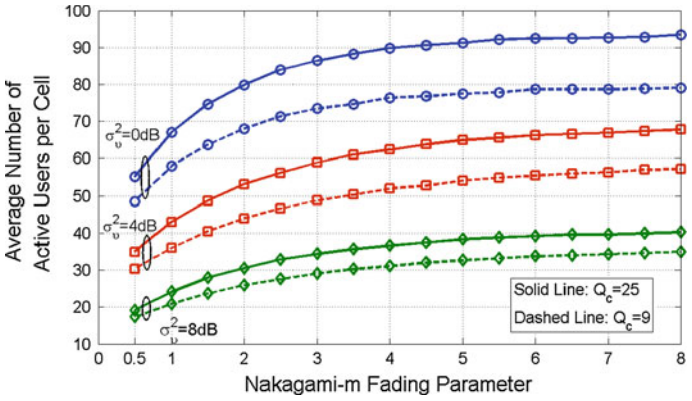

Fig. 10 Capacity (for a required $p_b = 0.01$) versus the Nakagami-m fading parameter for different values of σ_υ^2 and Q_c

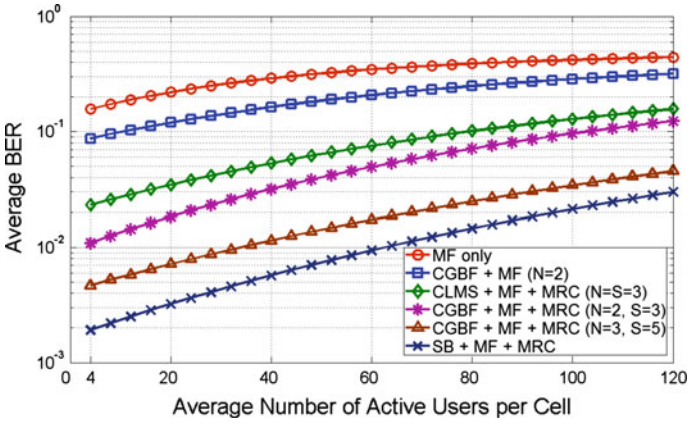

Fig. 11 Average BER versus the average number of active users per cell for different receivers

at a BER of 0.2, the number of users allowed in any cell is $K = 15$ users with the one-stage RAKE receiver, while with the two-stage RAKE receiver the number of users is $K = 57$ users. In addition, we can see that the average BER with the CLMS algorithm is higher than that with the CGBF algorithm. For example, at a BER of 0.1 and $S = 3$, the three-stage RAKE receiver for CGBF algorithm support $K = 103$ users, while it can support $K = 80$ users with CLMS algorithm. Also, we observe that the average BER for the SB technique is lower than that for the CGBF algorithm. For example, at a BER of 0.01, the three-stage RAKE receiver support $K = 34$ users for CGBF algorithm (for $N = 3$), while for SB technique, it can support $K = 63$ users. On the other hand, it can be seen that if N increases from 2 to 3, the number of active users in any cell for the three-stage RAKE receiver with CGBF algorithm increases from $K = 23$ users to $K = 67$ users for a required average BER of 0.02.

7 Conclusions

In this paper, we studied the RAKE receiver performance of multiple-cell DS-CDMA system with the space diversity processing, PCE, and voice activity in frequency-selective Nakagami fading channels. This receiver consists of CGBF, MF, and MRC in three stages. The way in which the Nakagami-m fading parameter, the average signal strength, the rate of average power decay, the processing gain, the PCE, the number of rake fingers, and the number of resolvable paths affect the reverse link capacity of the system has been discussed in detail.

In agreement with the results presented by Femenias and Carrasco [4] and Efthymoglou et al. [27], it has also been showed that for the number of rake fingers $L_r < L'$, the use of cell selection diversity as well as adaptive beamforming increases the effects of PCE on the average BER. However, the relative increased average BER degradation due to PCE, when using adaptive beamforming in conjunction with rake diversity combining and cell-selection diversity, does not directly translate into a relative increased capacity degradation of the system. While, in this paper we showed that for $L' \leq L_r \leq L$, the relative increased average BER degradation directly translates into a relative increased capacity degradation of the system. We also showed that for $L_r < L'$, better BER is achieved for $\Delta = 0.2$ than $\Delta = 0.0$, whereas the result is reversed for $L' \leq L_r \leq L$. In addition, the results indicate that in the presence of PCE, the effect of Nakagami fading channel parameters cannot be ignored in the performance analysis of DS-CDMA system. On the other hand, we have shown that average signal strength parameter Ω_0 in Nakagami fading channel affects the performance of the system. Accordingly, in this paper we showed that L' decreases as the average signal strength decreases.

It has also been observed that increasing the number of BSs in the cell-selection process Q_c improves the system capacity. In addition, our results showed that the variations in power level due to imperfections in power control have a detrimental effect on system performance. With a processing gain of 128, it was observed that a variance of 4 dB in power level results in a 43–46% capacity reduction (for $Q_c = 9$ and $Q_c = 25$) in terms of average error rate when the required BER is 0.01.

On the other hand, in agreement with the results presented by the authors [26], it has been observed that the average BER in the CGBF algorithm is lower than that in the CLMS algorithm, because in CGBF algorithm the IPI is removed whereas in CLMS algorithm it is not canceled. It has also been shown that the average BER in the SB technique is lower than that in the CGBF algorithm.

Appendix A

In this section, we present (41). Using (12), we have [4]

$$\omega_{s_x} = \mathrm{E}\left[\frac{1}{K}\sum_{k\in s_x}\Gamma_k(x,y)\right] = \begin{cases} 1; & S_x = S_{BS0} \\ \mathrm{E}\left[\mathrm{e}^{\xi_{s_0}^{(k)}}\right]\mathrm{E}\left[\chi_{F_{k0}}\right]\mathrm{E}\left[\frac{1}{\chi_{F_{kq}}}\right]; & S_x = S_{\overline{\mathrm{BS0}}} \\ \mathrm{E}\left[\mathrm{e}^{\xi_{s_1}^{(k)}}\right]\mathrm{E}\left[\chi_{F_{k0}}\right]\mathrm{E}\left[\frac{1}{\chi_{F_{kq}}}\right]; & S_x = S_1 \end{cases} \tag{A1}$$

with the parameters

$$\xi_{s_0}^{(k)} = -\beta\xi_{k,0} + \min_{\substack{q\in\Theta_k \\ q\neq 0}}\left\{\alpha \ln\frac{d_{k,q}}{d_{k,0}} + \beta\xi_{k,q}\right\} \tag{A2}$$

$$\xi_{s_1}^{(k)} = -\beta\xi_{k,0} + \min_{q\in\Theta_k}\left\{\alpha \ln\frac{d_{k,q}}{d_{k,0}} + \beta\xi_{k,q}\right\} \tag{A3}$$

also using (2), we have [10]

$$\mathrm{E}\left[\chi_{F_{k0}}\right] = \int_0^\infty x f_{\chi_F}(x)dx = 1 \tag{A4}$$

$$\mathrm{E}\left[\frac{1}{\chi_{F_{kq}}}\right] = \int_0^\infty \frac{1}{x} f_{\chi_F}(x)dx = \frac{L}{L-1} \tag{A5}$$

Substituting (A4) and (A5) into (A1), we have

$$\omega_{s_x} = \begin{cases} 1; & S_x = S_{BS0} \\ \frac{L}{L-1}\iint\limits_{s_0} E\left[\exp\left(\xi_{s_0}^{(k)}\right)\middle|\, \xi_{s_0}^{(k)} < 0\right] dA_0; & S_x = S_{\overline{\mathrm{BS0}}} \\ \frac{L}{L-1}\iint\limits_{s_1} E\left[\exp\left(\xi_{s_1}^{(k)}\right)\right] dA_1; & S_x = S_1 \end{cases} \tag{A6}$$

where A_0 and A_1 are the areas of regions S_0 and S_1, respectively. Using [4], the terms in the integral are found to be given by

$$E\left[\exp\left(\xi_{s_0}^{(k)}\right)\middle|\, \xi_{s_0}^{(k)} < 0\right] = e^{\beta^2\sigma_s^2} \sum_{\substack{q\in\Theta_k \\ q\neq 0}} \left(\frac{d_{k,q}}{d_{k,0}}\right)^\alpha \int_{-\infty}^{\infty} \frac{e^{-z^2/2}}{\sqrt{2\pi}} Q\left(z + \frac{\alpha}{\beta\sigma_s}\ln\frac{d_{k,q}}{d_{k,0}} + 2\beta\sigma_s\right) \times \prod_{\substack{q'\in\Theta_k \\ q'\neq 0, q'\neq q}} Q\left(z + \frac{\alpha}{\beta\sigma_s}\ln\frac{d_{k,q}}{d_{k,q'}} + \beta\sigma_s\right) dz \tag{A7}$$

$$E\left[\exp\left(\xi_{s_1}^{(k)}\right)\right] = e^{\beta^2\sigma_s^2} \sum_{q\in\Theta_k} \left(\frac{d_{k,q}}{d_{k,0}}\right)^\alpha \int_{-\infty}^{\infty} \frac{e^{-z^2/2}}{\sqrt{2\pi}} \prod_{\substack{q'\in\Theta_k \\ q'\neq q}} \times Q\left(z + \frac{\alpha}{\beta\sigma_s}\ln\frac{d_{k,q}}{d_{k,q'}} + \beta\sigma_s\right) dz \tag{A8}$$

References

1. Gejji, R. R. (1992). Forward-link-power control in CDMA cellular systems. *IEEE Transactions on Vehicular Technology, 41*(4), 532–536.
2. Abrardo, A., & Sennati, D. (2000). On the analytical evaluation of closed-loop power-control error statistics in DS-CDMA cellular systems. *IEEE Transactions on Vehicular Technology, 49*(6), 2071–2080.
3. Carrasco, L., & Femenias, G. (2008). Reverse link performance of a DS-CDMA system with both fast and slow power controlled users. *IEEE Transactions on Wireless Communications, 7*(4), 1255–1263.
4. Femenias, G., & Carrasco, L. (2006). Effect of slow power control error on the reverse link of OSTBC DS-CDMA in a cellular system with Nakagami frequency-selective MIMO fading. *IEEE Transactions on Vehicular Technology, 55*(6), 1927–1934.
5. Qian, L., & Gajic, Z. (2006). Variance minimization stochastic power control in CDMA system. *IEEE Transactions on Wireless Communications, 5*(1), 193–202.
6. Rintamaki, M., Koivo, H., & Hartimo, I. (2004). Adaptive closed-loop power control algorithms for CDMA cellular communication systems. *IEEE Transactions on Vehicular Technology, 53*(6), 1756–1768.

7. Wang, J., & Yu, A. (2001). Open-loop power control error in cellular CDMA overlay systems. *IEEE Journal on Selected Areas in Communications, 19*(7), 1246–1254.
8. Tam, W.-M., & Lau, F. C. M. (1999). Analysis of power control and its imperfections in CDMA cellular systems. *IEEE Transactions on Vehicular Technology, 48*(5), 1706–1717.
9. Newson, P., & Heath, M. R. (1994). The capacity of a spread spectrum CDMA system for cellular mobile radio with consideration of system imperfections. *IEEE Journal on Selected Areas in Communications, 12*(4), 673–684.
10. Romero-Jerez, J. M., Tellez-Labao, C., & Diaz-Estrella, A. (2004). Effect of power control imperfections on the reverse link of cellular CDMA networks under multipath fading. *IEEE Transactions on Vehicular Technology, 53*(1), 61–71.
11. Jansen, M. G., & Prasad, R. (1995). Capacity, throughput, and delay analysis of a cellular DS CDMA system with imperfect power control and imperfect sectorization. *IEEE Transactions on Vehicular Technology, 44*(1), 67–74.
12. Wang, J. T. (2009). Admission control with distributed joint diversity and power control for wireless networks. *IEEE Transactions on Vehicular Technology, 58*(1), 409–419.
13. Kumatani, K., McDonough, J., Rauch, B., Klakow, D., Garner, P. N., & Li, W. (2009). Beamforming with a maximum negentropy criterion. *IEEE Transactions on Audio, Speech, and Language Processing, 17*(5), 994–1008.
14. Zhang, R., Chai, C. C., & Liang, Y. (2009). Joint beamforming and power control for multiantenna relay broadcast channel with QoS constraints. *IEEE Transactions on Signal Processing, 57*(2), 726–737.
15. Chang, J., Tassiulas, L., & Rashid-Farrokhi, F. (2002). Joint transmitter receiver diversity for efficient space division multiaccess. *IEEE Transactions on Wireless Communications, 1*(1), 16–27.
16. Abrardo, A. (2003). Noncoherent MLSE in DS-CDMA wireless systems with antenna arrays. *IEEE Transactions on Vehicular Technology, 52*(6), 1435–1446.
17. Yang, L.-L., & Fang, W. (2009). Performance of distributed-antenna DS-CDMA systems over composite lognormal shadowing and Nakagami-*m*-fading channels. *IEEE Transactions on Vehicular Technology, 58*(6), 2872–2883.
18. Cai, Y., & de Lamare, R. C. (2009). Space-time adaptive MMSE multiuser decision feedback detectors with multiple-feedback interference cancellation for CDMA systems. *IEEE Transactions on Vehicular Technology, 58*(8), 4129–4140.
19. Abdel-Samad, A., Davidson, T. N., & Gershman, A. B. (2006). Robust transmit eigen beamforming based on imperfect channel state information. *IEEE Transactions on Signal Processing, 54*(5), 1596–1609.
20. Wang, J., & Payaro, M. (2010). On the robustness of transmit beamforming. *IEEE Transactions on Signal Processing, 58*(11), 5933–5938.
21. Nai, S. E., Ser, W., Yu, Z. L., & Rahardja, S. (2009). A robust adaptive beamforming framework with beampattern shaping constraints. *IEEE Transactions on Antennas and Propagation, 57*(7), 2198–2203.
22. El-Keyi, A., & Champagne, B. (2010). Adaptive linearly constrained minimum variance beamforming for multiuser cooperative relaying using kalman filter. *IEEE Transactions on Wireless Communications, 9*(2), 641–651.
23. Lorenz, R. G., & Boyd, S. P. (2005). Robust minimum variance beamforming. *IEEE Transactions on Signal Processing, 53*(5), 1684–1696.
24. Lawrence, D. E. (2010). Low probability of intercept antenna array beamforming. *IEEE Transactions on Antennas and Propagation, 58*(9), 2858–2865.
25. Park, S.-H., Lee, H., Lee, S.-R., & Lee, I. (2009). A new beamforming structure based on transmit-MRC for closed-loop MIMO systems. *IEEE Transactions on Communications, 57*(6), 1847–1856.
26. Dosaranian-Moghadam, M., Bakhshi, H., & Dadashzadeh, G. (2011). Reverse link performance of DS-CDMA cellular systems through closed-loop power control, base station, and antenna arrays in 2D urban environment. *Wireless Personal Communications*. doi:10.1007/s11277-011-0250-6.
27. Efthymoglou, G. P., Aalo, V. A., & Helmken, H. (1997). Performance analysis of coherent DS-CDMA systems in a Nakagami fading channel with arbitrary parameters. *IEEE Transactions on Vehicular Technology, 46*(2), 289–297.
28. Rashid-Farrokhi, F., Ray-Liu, K. J., & Tassiulas, L. (1998). Transmit beamforming and power control for cellular systems. *IEEE Journal on Selected Areas in Communications, 16*(8), 1437–1450.
29. Mohamed, N. A., & Dunham, J. G. (2002). A low-complexity combined antenna array and interference cancellation DS-CDMA receiver in multipath fading channels. *IEEE Journal on Selected Areas in Communications, 20*(2), 248–256.
30. Mohamed, N. A., & Dunham, J. G. (1999). Adaptive beamforming for DS-CDMA using conjugate gradient algorithm in a multipath fading channel. In *Proceedings of the 1999 IEEE emerging technologies symposium*, Dallas, TX (pp. 859–863)

31. Dosaranian-Moghadam, M., Bakhshi, H., & Dadashzadeh, G. (2010). Interference management for DS-CDMA receiver through base station assignment in multipath fading channels. In *Proceedings of the 2010 IEEE international conference on wireless communications, networking and information security*, Beijing, China (pp. 257–263). June 2010.
32. Dosaranian-Moghadam, M., Bakhshi, H., & Dadashzadeh, G., (2010). Adaptive beamforming method based on closed-loop power control for DS-CDMA receiver in multipath fading channel. In *21st annual IEEE international symposium on personal, indoor, and mobile radio communications*, Istanbul, Turkey (pp. 2087–2092). 26–30 September, 2010.
33. Litva, J., & Kwok-Yeung, T. (1996). *Digital beamforming in wireless communications*. Boston, London: Artech House.
34. Gradshteyn, I. S., & Ryzhik, I. M. (1996). *Table of integrals, series, and products* (6th ed.). San Diego, CA: Academic.
35. Alouini, M.-S., Abdi, A., & Kaveh, M. (2001). Sum of gamma variates and performance of wireless communication systems over Nakagami-fading channels. *IEEE Transactions on Vehicular Technology, 50*(6), 1471–1480.
36. Lei, X., & Fan, P. (2010). On the error performance of M-ary modulation schemes on Rician-Nakagami fading channels. *Wireless Personal Communications, 53*(4), 591–602.
37. Chen, J. I.-Z. (2005). Performance evaluation of multiple-cell DS-CDMA systems over correlated Nakagami-m fading environments. *Wireless Personal Communications, 33*(1), 21–34.
38. Oh, S. W., & Li, K. H. (2001). Performance evaluation for forward-link cellular DS-CDMA over frequency-selective Nakagami multipath fading channels. *Wireless Personal Communications, 18*(3), 275–287.
39. Peterson, R. L., Ziemer, R. E., & Borth, D. E. (1995). *Spread-spectrum communications*. Englewood Cliffs, NJ: Prentice-Hall.
40. Kong, N., & Milstein, L. B. (1999). Average SNR of a generalized diversity selection combining scheme. *IEEE Communications Letters, 3*(3), 57–59.
41. Holtzman, J. M. (1992). A simple, accurate method to calculate spread-spectrum multiple-access error probabilities. *IEEE Transactions on Communications, 40*(3), 461–464.
42. Dosaranian-Moghadam, M., Bakhshi, H., & Dadashzadeh, G. (2010). Interference management for DS-CDMA systems through closed-loop power control, base station assignment, and beamforming. *Journal of Wireless Sensor Network, 2*(6), 472–482.
43. Dosaranian-Moghadam, M., Bakhshi, H., Dadashzadeh, G., & Godarzvand-Chegini, M. (2010). Joint base station assignment, power control error, and adaptive beamforming for DS-CDMA cellular systems in multipath fading channels. In *Proceedings of the 2010 IEEE global mobile congress*, Shanghai, China (pp. 1–7). 18–19 October, 2010.
44. Dosaranian-Moghadam, M., Bakhshi, H., & Dadashzadeh, G. (2010). Joint constrained LMS algorithm and base station assignment for DS-CDMA receiver in multipath fading channels. In *Proceedings of the 2010 IEEE wireless communications, networking and mobile computing*, Chengdu, China (pp. 1–7). 23–25 September, 2010.
45. Liberti, J. C., & Rappaport, T. S. (1999). *Smart antennas for wireless communications IS-95 and third generation CDMA applications*. Englewood Cliffs, NJ: Prentice-Hall.
46. Sun, X. Y., Lian, X. H., & Zhou, J. J. (2008). Robust adaptive beamforming based on maximum likelihood estimation. In *Proceedings of the 2008 IEEE international conference on microwave and millimeter wave technology*, Nanjing, China (Vol. 3, pp. 1137–1140). 21–24 April, 2008.
47. Dosaranian-Moghadam, M., Bakhshi, H., Dadashzadeh, G., & Rahmati, P. (2009). Adaptive beamforming method based on constrained LMS algorithm for tracking mobile user. In *Proceedings of the 2009 IEEE global mobile congress*, Shanghai, China (pp. 1–6). October 2009.
48. Gotsis, K. A., Siakavara, K., & Sahalos, J. N. (2009). On the direction of arrival (DoA) estimation for a switched-beam antenna system using neural networks. *IEEE Transactions on Antennas and Propagation, 57*(5), 1399–1411.
49. Dosaranian-Moghadam, M., Bakhshi, H., & Dadashzadeh, G. (2010). Joint centralized power control and cell sectoring for interference management in CDMA cellular systems in a 2D urban environment. *Journal of Wireless Sensor Network, 2*(8), 599–605.

Author Biographies

Mohamad Dosaranian-Moghadam was born in Tehran, Iran on May 26, 1979. He received the B.Sc. degree in electrical engineering from Qazvin Branch of Islamic Azad University, Qazvin, Iran and the M.Sc. degree in communication engineering from Ferdowsi University, Mashad, Iran, in 2002 and 2005, respectively, and the Ph.D. degree in communication engineering from Department of Electrical Engineering, Science and Research Branch of Islamic Azad University, Tehran, Iran in 2011. He is currently as Assistance Professor in the Department of Electrical Engineering at Qazvin Branch of Islamic Azad University, Qazvin, Iran. His research interests include power control, wireless communications, array and statistical signal processing, smart antennas, and adaptive filtering.

Hamidreza Bakhshi was born in Tehran, Iran on April 25, 1971. He received the B.Sc. degree in electrical engineering from Tehran University, Iran in 1992, the M.Sc. and Ph.D. degree in Electrical Engineering from Tarbiat Modarres University, Iran in 1995 and 2001, respectively. He is currently as Associate Professor in the Department of Electrical Engineering at Shahed University, Tehran, Iran. His research interests include wireless communications, multiuser detection, and smart antennas.

Gholamreza Dadashzadeh was born in Urmia, Iran, in 1964. He received the B.Sc. degree in communication engineering from Shiraz University, Shiraz, Iran in 1992 and M.Sc. and Ph.D. degree in communication engineering from Tarbiat Modarres University (TMU), Tehran, Iran, in 1996 and 2002, respectively. From 1998 to 2003, he has worked as head researcher of Smart Antenna for Mobile Communication Systems (SAMCS) and WLAN 802.11 project in radio communications group of Iran Telecomm Research Center (ITRC). From 2004 to 2008, he was dean of Communications Technology Institute (CTI) in ITRC. He is currently as Assistance Professor in the Department of Electrical Engineering at Shahed University, Tehran, Iran. He is a member of IEEE, Institute of Electronics, Information and Communication Engineers (IEICE) of Japan and Iranian Association of Electrical and Electronics Engineers (IAEEE) of Iran. He honored received the first degree of national researcher in 2007 from Iran's ministry of ICT. He has published more than 50 papers in referred journals and international conferences in the area of antenna design and smart antennas.